Chinese Chemical Letters 34 (2023) 107852

Contents lists available at ScienceDirect

Chinese Chemical Letters

journal homepage: www.elsevier.com/locate/cclet

Hybrid diluents enable localized high-concentration electrolyte with balanced performance for high-voltage lithium-metal batteries

Chengzong Li[1], Yan Li[1], Ziyu Chen, Yongchao Zhou, Fengwei Bai, Tao Li*

School of Resource Environment and Safety Engineering, University of South China, Hengyang 421001, China

ARTICLE INFO

Article history:
Received 8 August 2022
Revised 2 September 2022
Accepted 22 September 2022
Available online 25 September 2022

Keywords:
Localized high-concentration electrolyte
High-voltage lithium-metal batteries
Solid electrolyte interphase
Electrolyte
Ion-transport kinetics

ABSTRACT

Localized high-concentration electrolytes (LHCE) have shown good compatibility with high-voltage lithium (Li)-metal batteries, but their practicality is yet to be proved in terms of cost and safety. Here we develop a hybrid-LHCE with favorable integrated properties by combining the merits of two representative diluents, fluorobenzene (FB) and 1,1,2,2-tetrafluoroethyl-2,2,2-trifluoroethyl ether (TFE). Specifically, the extremely cheap and lightweight FB significantly reduces the cost and density of electrolyte, while the fire-retardant TFE circumvents the flammable nature of FB and thus greatly improves the safety of electrolyte. Moreover, the FB–TFE mixture enhances the thermodynamic stability of hybrid-LHCE and renders a controllable defluorination of FB, contributing to the formation of a thin and durable inorganic-rich solid electrolyte interphase (SEI) with rapid ion-transport kinetics. Benefiting from the designed hybrid-LHCE, a Li|NCM523 battery demonstrates excellent cycling performance (215 cycles, 91% capacity retention) under challenging conditions of thin Li-anode (30 μm) and high cathode loading (3.5 mAh/cm^2).

Commercialized lithium (Li)-ion batteries are approaching their ceiling of energy density (300 Wh/kg at cell-level) [1]. To further increase the energy density, high-voltage Li-metal batteries (LMBs) with practical cell-level energy density of 350∼500 Wh/kg have been pursued as the next-generation power source [2–4]. However, the practical application of high-voltage LMBs is impeded by poor cycling life and safety hazard, which originates from the high reactivities of Li-metal with electrolytes [5–7]. The resulting inhomogeneous and fragile solid-electrolyte interphase (SEI) formed on Li-metal anode causes dendritic Li growth and dead Li formation, consuming both Li-metal and electrolyte rapidly [8–12]. Therefore, developing Li-metal anode compatible electrolytes is a prerequisite for the commercial implementation of high-voltage LMBs.

Several promising liquid electrolytes (fluorinated electrolytes [13–15], weakly solvating electrolytes [16–18], dual-salt electrolytes [7,19,20], additives-modified electrolytes [21–23], liquified gas electrolytes [24], high concentration electrolytes (HCE) [25–28], localized high concentration electrolytes (LHCE) [29,30], *etc.* [31,32]) have been designed to tune the SEI chemistry to minimize the uncontrollable side reactions between Li-metal anode and electrolyte. Among them, HCE and LHCE have shown superior compatibility with high-voltage LMBs due to the formation of anion-derived inorganic-rich electrolyte/electrode interphases, which offer both excellent stability and rapid ion-transport kinetics [33]. In comparison to HCE, LHCE shows better physical properties (such as low viscosity, good wettability and low cost) owning to the introduction of an inert diluent (also called non-solvating cosolvent). Despite its inertness, the choice of diluent for LHCE is crucial. Ideally, diluent should possess several features, such as low viscosity, sufficient electrochemical stability, appropriate miscibility, and poor solvating capability [34]. Hydrofluoroethers (HFEs), including bis(2,2,2-trifluoroethyl) ether (BTFE) [29], 1,1,2,2-tetrafluoroethyl-2,2,3,3-tetrafluoropropyl ether (TTE) [30], 1,1,2,2-tetrafluoroethyl-2,2,2-trifluoroethyl ether (TFE) [35], and hexafluoroisopropyl-methyl ether (HFME) [36], possess the above features and are widely used as diluents [37]. However, the high cost and high density (>1.4 g/cm^3) of the highly fluorinated HFEs increases the cost and compromises the energy density of LMBs.

In this regard, fluorinated aromatics with low degree of fluorination, such as fluorobenzene (FB) [38,39], 1,2-difluorobenzene (1,2-dFB) [40], trifluoromethoxybenzene (TFMB) [41], and trifluoromethylbenzene (BZTF) [42], have been adopted as diluents for LHCE because of its low cost and low density. Generally, fluorinated aromatics are F-donating diluents and the trend to defluorination varies greatly, while HFEs are much inert and do not participate in the formation of SEI. However, the electrochemical or thermodynamic stability of some fluorinated aromatics need to

* Corresponding author.
E-mail address: li-tao@usc.edu.cn (T. Li).
[1] These authors contributed equally to this work.

https://doi.org/10.1016/j.cclet.2022.107852
1001-8417/

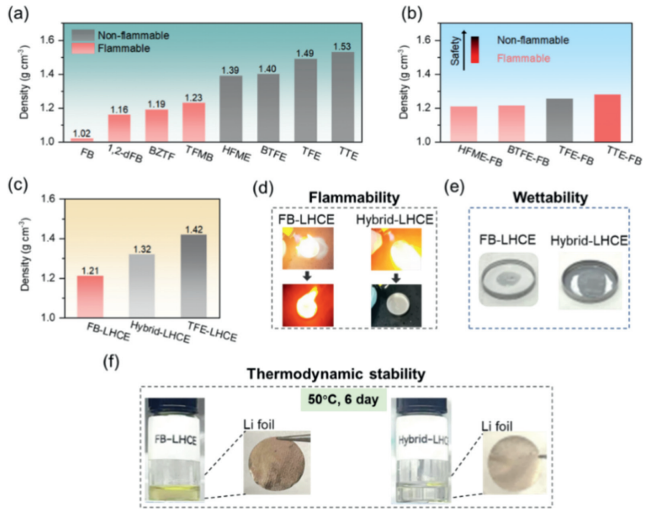

Fig. 1. (a) Summary of density and flammability of common diluents. (b) Flammability of different HFE–FB combinations. (c) Density of the three LHCE. (d) Ignition test of FB-LHCE and hybrid-LHCE. (e) Wettability of different LHCE to separator. (f) Images of different LHCE and the immersed Li foils after 6 days storage at 50 °C.

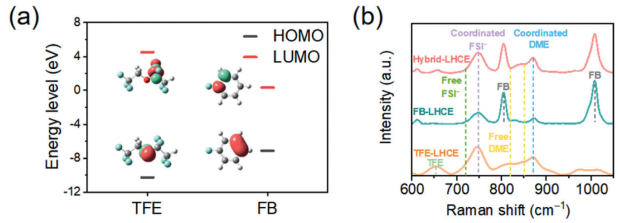

Fig. 2. (a) Energy level and visual HOMOs and LUMOs of TFE and FB. The red and green regions represent the positive and negative parts of orbitals, respectively. Color mapping for elements: H-white, C-grey, O-red, F-cyan. (b) Raman spectra of FB-LHCE, TFE-LHCE and hybrid-LHCE.

be improved. For example, FB-LHCE is insufficient to support high-operating voltage and 1,2-dFB exhibits relative high reactivity with Li-metal [41,43]. Moreover, these fluorinated aromatics are highly flammable. Thus, it is challenging yet highly desirable to design a LHCE with favorable integrated properties (low cost, low density, nonflammability, high electrochemical stability, *etc.*).

Herein, we present a hybrid-LHCE employing FB–TFE mixture (1:1, v/v) as diluent, which demonstrates balanced properties (such as nonflammability, low-cost and moderate density). Specifically, the extremely cheap and lightweight FB can significantly reduce the cost and density of hybrid-LHCE, while the fire retardant TFE circumvents the flammable nature of FB and thus greatly improves the safety of hybrid-LHCE. Moreover, the FB–TFE mixture enhances the thermodynamic stability of hybrid-LHCE, leading to less parasitic reactions with Li-metal in comparison to FB-LHCE. In the presence of TFE with higher LUMO level and lower HOMO level, the defluorination of FB proceeds in a more controllable way. The resulting thin and durable inorganic-rich SEI effectively suppresses the side reactions between Li-metal and electrolyte, thus significantly improving the cycling reversibility of Li-metal anode. Notably, Li|NCM523 battery cycled with hybrid-LHCE achieved a capacity retention of 91% after 215 cycles under challenging conditions of thin Li-anode (30 μm) and high cathode loading (3.5 mAh/cm^2). This work offers a simple and feasible design principle for constructing LHCE with balanced performances for high-energy LMBs.

The physiochemical properties (flammability, density, wettability, *etc.*) of LHCE greatly depend on the diluent because of its large volume ratio (>50%). Hence the choice of diluent for LHCE is critical. The flammability, density and molecular structures of common diluents are summarized in Fig. 1a and Fig. S1 (Supporting information). FB possesses the merits of low density (1.02 g/cm^3) and low cost compared with HFEs, but it is highly flammable. To construct a nonflammable and lightweight LHCE, HFE–FB combination (1:1 by volume) is used as hybrid diluents. Among the designed HFE–FB combinations (HFME–FB, BTFE–FB, TFE–FB, and TTE–FB), TFE–FB successfully circumvents the flammable nature of FB (Fig. 1b and Table S1 in Supporting information), which is possibly associated with the highest F/C ratio of TFE among the studied HFEs. Thus, TFE–FB combination was chosen as hybrid diluents to prepare LHCE. Three LHCE were prepared, *i.e.*, 2.0 mol/L LiFSI/DME/FB/TFE (1/1.2/1.1/1.6 by mol, denoted as hybrid-LHCE), 2.0 mol/L LiFSI/DME/FB (1/1.2/3.2 by mol, denoted as FB-LHCE), and 2.0 mol/L LiFSI/ DME/TFE (1/1.2/2.2 by mol, denoted as TFE-LHCE). The hybrid-LHCE shows a medium density of 1.32 g/cm^3 among the three LHCE (Fig. 1c). A reduction of 7% in electrolyte weight per volume and an increase of 3% in energy density can be achieved using hybrid-LHCE relative to TFE-LHCE (Fig. S2 in Supporting information). As expected, hybrid-LHCE and TFE-LHCE did not burn after ignition while FB-LHCE was easily ignited by the flame (Fig. 1d and Fig. S3 in Supporting information). Besides, the wettability of hybrid-LHCE to separator is better than that of FB-LHCE (Fig. 1e). The superior wettability of hybrid-LHCE contributes to uniform electrolyte distribution in practical application. Thermodynamic stability of hybrid-LHCE was investigated by storing the electrolyte at 50 °C for 6 days. As shown in Fig. 1f, FB-LHCE and the immersed Li foil turned yellow and black, respectively, which is due to the spontaneously happened parasitic reactions. In contrast, both hybrid-LHCE and the immersed Li foil exhibited no apparent change in appearance after storage, indicating its superior thermodynamic stability. The improved thermodynamic stability of hybrid-LHCE against Li metal was further evidenced by the less increase in cell impedance during calendar ageing (Fig. S4 in Supporting information). Thus, a hybrid-LHCE with balanced properties (such as nonflammability, low-cost, and moderate density) has been successfully developed by employing FB–TFE mixture (1:1, v/v) as diluent.

The electrochemical stability of TFE and FB is evaluated by the energy values of their LUMO and HOMO. FB exhibits a higher energy level of HOMO and lower energy level of LUMO than TFE (Fig. 2a), indicating that FB is prone to decomposition at both Li-metal anode and high-voltage cathode and participate in the formation of SEI and CEI. Thus, hybrid-LHCE is expected to decompose in a milder way in comparison to FB-LHCE. The solvation structure of the three LHCE were probed by Raman spectroscopy (Fig. 2b). The three LHCE (FB-LHCE, TFE-LHCE, hybrid-LHCE) exhibit the same vibration band at 750 and 870 cm^{-1} assigned to coordinated FSI^- and DME, respectively, suggesting that the diluents have negligible influence on the Li^+-FSI^--DME solvate.

The reversibility of Li plating/stripping in FB-LHCE and hybrid-LHCE was evaluated by measuring the Columbic efficiency (CE) of Li|Cu half cells. As shown in Figs. 3a and b, hybrid-LHCE shows a higher CE (99.7%) and lower overpotential than that of FB-LHCE (99.6%), suggesting that a more uniform and durable SEI was derived from hybrid-LHCE. The practicability of hybrid-LHCE was further evaluated in Li|NCM523 full cells under challenging conditions of thin Li-anode (30 μm) and high loading cathode (3.5 mAh/cm^2). As shown in Fig. 3c, Li|NCM523 batteries with FB-LHCE experienced a rapid decay in capacity after 110 cycles, which is attributed to the fast depletion of Li-metal (Fig. S5 in Supporting information). In contrast, ~170 stable cycles was achieved in the case of TFE-LHCE, indicating that the electrochemical inert TFE is superior to FB in constructing stable LHCE for high-voltage LMBs (Fig. S6 in Supporting information). Notably, a significantly prolonged cycling

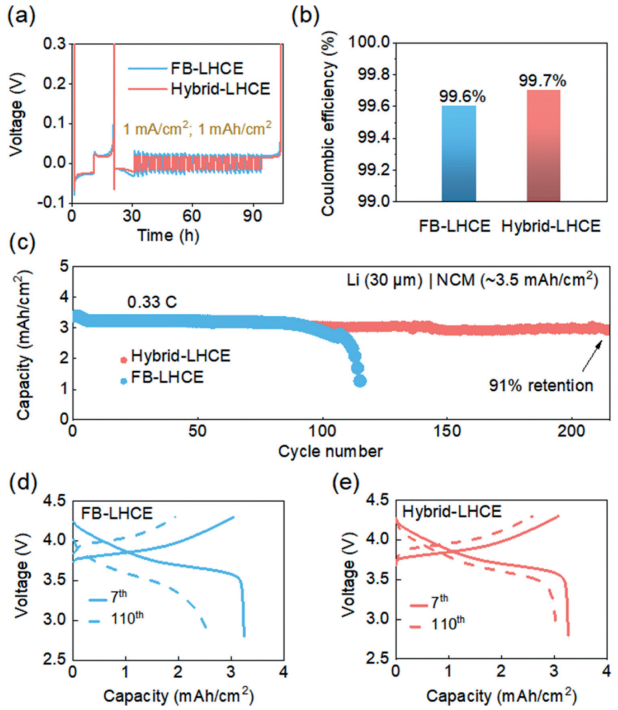

Fig. 3. (a, b) CE of Li|Cu half cells using different electrolytes. (c) Cycling performance of Li|NCM523 full cells with FB-LHCE and hybrid-LHCE at 0.33 C after seven formation cycles. Corresponding charge/discharge curves of Li|NCM523 full cells cycled in (d) FB-LHCE and (e) hybrid-LHCE.

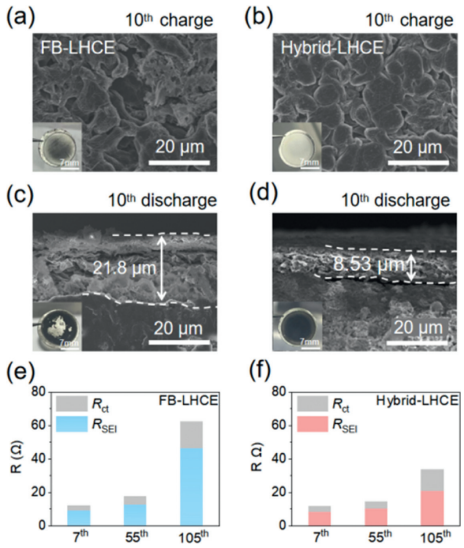

Fig. 4. Li deposition morphology in (a) FB-LHCE and (b) hybrid-LHCE at the 10th deposition. The Li anodes were retrieved from Li|NCM523 batteries (at the 10th charge state). Cross-sectional views of cycled Li anodes retrieved from Li|NCM523 batteries (at the 10th discharge state) with (c) FB-LHCE and (d) hybrid-LHCE. The evolution of interfacial resistance of Li|NCM523 batteries with (e) FB-LHCE and (f) hybrid-LHCE.

life (215 cycles, 91% capacity retention) was achieved in hybrid-LHCE. Besides, the increase of cell overpotentials upon cycling in Li|NCM523 batteries with hybrid-LHCE was significantly inhibited compared to FB-LHCE (Figs. 2d and e). The above results indicate the possible synergistic effect between FB and TFE and demonstrate the effectiveness and practicability of hybrid-LHCE in improving the lifespan of high-voltage LMBs.

Li deposition morphology was examined by scanning electron microscopy (SEM) to provide a clue to the improved cycling performance of hybrid-LHCE. Li-anodes for SEM characterization were retrieved from Li|NCM523 batteries after 10 cycles. Irregular nodule-like Li deposits covered with porous SEI residues were observed in FB-LHCE (Fig. 4a). Such a loose structure readily allows for side reactions with electrolyte and is susceptible to dead Li formation during the stripping process, as evidenced by the optical image of the cycled Li-anode (Fig. 4 inset a). In contrast, compact Li granules with a clear surface were formed in hybrid-LHCE (Fig. 4b). Besides, no obvious dead Li and SEI residues were observed on the cycled Li-anode (Fig. 4b inset), suggesting that a more uniform and durable SEI layer was formed in hybrid-LHCE. The much thinner layer of dead Li reconfirms that less parasitical reactions generate in hybrid-LHCE (Figs. 4c and d). The interfacial resistance evolution of Li|NCM523 batteries with FB-LHCE and hybrid-LHCE was investigated by electrochemical impedance spectroscopy (EIS). The values of interfacial resistances, including surface film resistance (R_{SEI}) and charge transfer (R_{ct}), were obtained by fitting the semicircles in the high and middle frequency regions according to the equivalent circuit (Fig. S7 in Supporting information). The interfacial resistance of Li|NCM523 batteries with FB-LHCE showed a significant increase (408%) from the 7th to 105th cycles (Fig. 4e, Fig. S7 and Table S2 in Supporting information), indicating the accumulation of a thick layer of dead Li as well as the deteriorated Li^+ transport kinetics in SEI. In contrast, the value increased by only 190% in the case of hybrid-LHCE (Fig. 4f, Fig. S7 and Table S2), verifying the formation of an efficient and durable SEI.

The chemical components of SEI derived from FB-LHCE and hybrid-LHCE were analyzed by X-ray photoelectron spectroscopy (XPS). The strong C–H/C–C peak at 284.8 eV in the C 1s spectrum suggested that the SEI featured an organic-rich outer layer (Figs. 5a and b). The high ratio of Li–C peak along with the ultra-high atomic ratio of Li (>70%) revealed that a much thinner SEI was formed in hybrid-LHCE compared to FB-LHCE (Figs. 5a-c). After etching for 240 s, a weaker LiF peak and much lower F/N ratio were observed in the hybrid-LHCE-derived SEI, indicating the defluorination of FB is more controllable in hybrid-LHCE (Figs. 5a and b, Fig. S8 in Supporting information). For O-containing species, the hybrid-LHCE-derived SEI was mainly composed of Li_2O, while in the FB-LHCE-derived SEI, the organic COOR species accounted for a considerable ratio (Figs. 5a and b). The chemical components of SEI after etching are summarized in Fig. 5d. The ratio of inorganic components in hybrid-LHCE-derived SEI is significantly higher than that in FB-LHCE-derived SEI. These inorganics (LiF, Li_2O, Li_2CO_3, Li_3N, *etc.*) are beneficial to improving the ion-transport kinetics of SEI [44–47]. The accelerated ion-transport kinetics in hybrid-LHCE-derived SEI was further evidenced by its larger exchange current density (0.26 mA/cm^2) than that of FB-LHCE-derived SEI (0.08 mA/cm^2) (Fig. 5e). Thus, such a thin and inorganic-rich SEI formed in hybrid-LHCE is responsible for the improved cycling stability of Li|NCM523 batteries. On the cathode side, the defluorination of FB is also mitigated in hybrid-LHCE, as confirmed by the much weaker LiF peak in the hybrid-LHCE derived CEI (Fig. 5f). Therefore, the controllable defluorination of FB at both Li-anode and NCM523 cathode contributed to the formation of a sustainable and efficient electrode/electrolyte interphases

In summary, a hybrid-LHCE with favorable integrated properties (such as nonflammable, low-cost, and lightweight) is developed by combining the merits of two representative types of diluents, hydrofluoroether and fluorinated aromatics. Concretely, the nonflammable TFE greatly improves the safety of hybrid-LHCE, while the cheap and lightweight FB can reduce the cost and density of hybrid-LHCE. Moreover, the introduction of TFE enhances the thermodynamic stability of hybrid-LHCE, leading to less parasitic reactions with Li-metal in comparison to FB-LHCE. In the presence of electrochemically stable TFE, the defluorination of FB proceeds in a more controllable way, contributing to the formation of a thinner

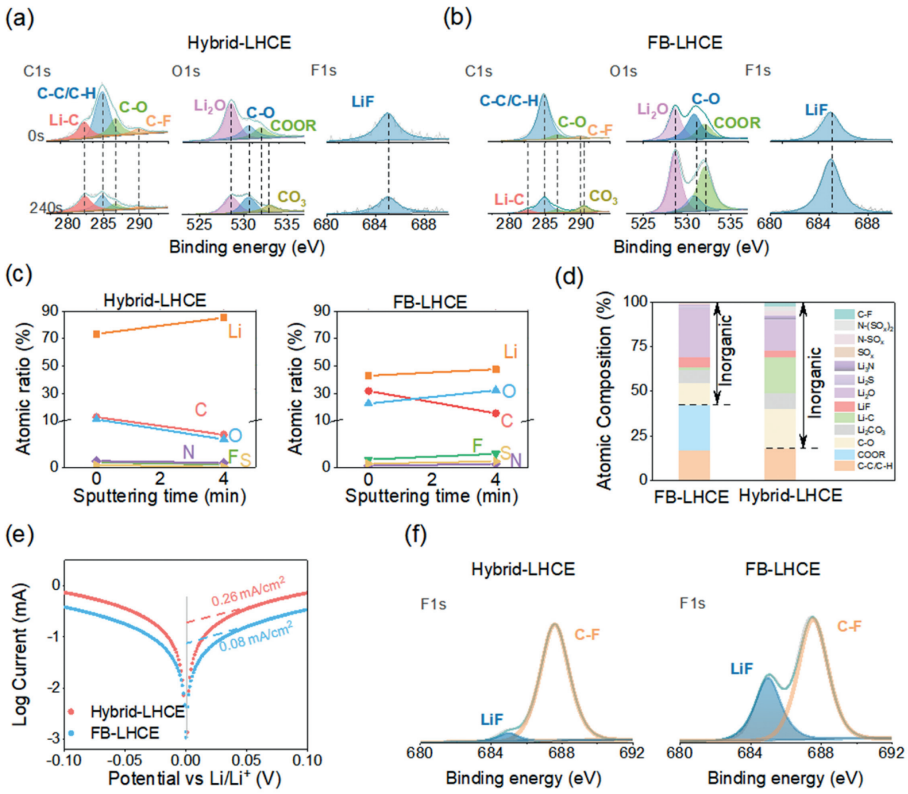

Fig. 5. C 1s, O 1s and F 1s depth profiles of SEI formed in (a) hybrid-LHCE and (b) FB-LHCE. The Li-metal anodes for XPS analysis were retrieved from Li|NCM523 batteries at the first charge state. (c) The atomic ratios of Li, O, C, F, S and N in SEI formed in different electrolytes. (d) Quantified chemical components of SEI after etching. The components ratios were calculated from the fitted peak areas. (e) Tafel plots and the calculated values of exchange current density in different electrolytes. (f) F 1s spectrum of CEI formed in (a) hybrid-LHCE and (b) FB-LHCE. The NCM523 cathodes for XPS analysis were retrieved from Li|NCM523 cells at charge state after 10 cycles.

and durable inorganic-rich electrode/electrolyte interphases. Benefiting from the favorable integrated properties of hybrid-LHCE, the Li|NCM523 battery achieves a capacity retention of 91% after 215 cycles under challenging conditions of thin Li-anode (30 μm) and high cathode loading (3.5 mAh/cm^2). This study demonstrates that employing different types of diluents with specific merits is a feasible strategy to design high performance LHCE for high-energy Li-metal batteries.

Declaration of competing interest

The authors declare that they have no known competing financial interests or personal relationships that could have appeared to influence the work reported in this paper.

Acknowledgments

This work was supported by the National Natural Science Foundation of China (No. 21808125), China Postdoctoral Science Foundation (No. 2020M672805). The theoretical calculations were supported by Tsinghua National Laboratory for Information Science and Technology. We thank Xiang Chen (Tsinghua University) for kindly providing the theoretical calculation results.

Supplementary materials

Supplementary material associated with this article can be found, in the online version, at doi:10.1016/j.cclet.2022.107852.

References

[1] M. Li, J. Lu, Z. Chen, K. Amine, Adv. Mater. 30 (2018) 1800561.
[2] J. Liu, Z. Bao, Y. Cui, et al., Nat. Energy 4 (2019) 180–186.
[3] C. Niu, D. Liu, J.A. Lochala, et al., Nat. Energy 6 (2021) 723–732.
[4] X.B. Cheng, R. Zhang, C.Z. Zhao, Q. Zhang, Chem. Rev. 117 (2017) 10403–10473.
[5] K. Xu, Chem. Rev. 114 (2014) 11503–11618.
[6] P. Albertus, S. Babinec, S. Litzelman, A. Newman, Nat. Energy 3 (2017) 16–21.
[7] R. Xu, X. Shen, X.X. Ma, et al., Angew. Chem. Int. Ed. 60 (2021) 4215–4220.
[8] H. Wu, H. Jia, C. Wang, J.G. Zhang, W. Xu, Adv. Energy Mater. 11 (2021) 2003092.
[9] C. Yan, H. Yuan, H.S. Park, J.Q. Huang, J. Energy Chem. 47 (2020) 217–220.
[10] X.R. Chen, C. Yan, J.F. Ding, H.J. Peng, Q. Zhang, J. Energy Chem. 62 (2021) 289–294.
[11] J.F. Ding, R. Xu, C. Yan, et al., J. Energy Chem. 59 (2021) 306–319.
[12] M.Y. Zhou, X.Q. Ding, J.F. Ding, et al., Joule 6 (2022) 2122–2137.
[13] X. Fan, X. Ji, L. Chen, et al., Nat. Energy 4 (2019) 882–890.
[14] X. Fan, L. Chen, O. Borodin, et al., Nat. Nanotechnol. 13 (2018) 715–722.
[15] L. Suo, W. Xue, M. Gobet, et al., Proc. Natl. Acad. Sci. U. S. A. 115 (2018) 1156–1161.
[16] Y.X. Yao, X. Chen, C. Yan, et al., Angew. Chem. Int. Ed. 60 (2021) 4090–4097.
[17] C.V. Amanchukwu, X. Kong, J. Qin, Y. Cui, Z. Bao, Adv. Energy Mater. 9 (2019) 1902116.
[18] R. Xu, J.F. Ding, X.X. Ma, et al., Adv. Mater. 33 (2021) 2105962.
[19] R. Weber, M. Genovese, A.J. Louli, et al., Nat. Energy 4 (2019) 683–689.
[20] J. Zheng, M.H. Engelhard, D. Mei, et al., Nat. Energy 2 (2017) 17012.
[21] Y. Liu, D. Lin, Y. Li, et al., Nat. Commun. 9 (2018) 3656.
[22] T. Li, X.Q. Zhang, N. Yao, et al., Angew. Chem. Int. Ed. 60 (2021) 22683–22687.
[23] S. Li, W. Zhang, Q. Wu, et al., Angew. Chem. Int. Ed. 59 (2020) 14935–14941.
[24] Y. Yin, Y. Yang, D. Cheng, et al., Nat. Energy 7 (2022) 548–559.
[25] J. Qian, W.A. Henderson, W. Xu, et al., Nat. Commun. 6 (2015) 6362.
[26] K. Yoshida, M. Nakamura, Y. Kazue, et al., J. Am. Chem. Soc. 133 (2011) 13121–13129.
[27] C. Wu, Y. Zhou, X. Zhu, et al., Acta Phys. Chim. Sin. 37 (2021) 2008044.
[28] O. Borodin, J. Self, K.A. Persson, C. Wang, K. Xu, Joule 4 (2020) 69–100.
[29] S. Chen, J. Zheng, D. Mei, et al., Adv. Mater. 30 (2018) 1706102.
[30] X. Ren, L. Zou, X. Cao, et al., Joule 3 (2019) 1662–1676.
[31] W. Wu, Y. Bai, X. Wang, C. Wu, Chin. Chem. Lett. 32 (2021) 1309–1315.
[32] S. Zhang, B. Cheng, Y. Fang, et al., Chin. Chem. Lett. 33 (2022) 3951–3954.
[33] Y. Xiao, R. Xu, L. Xu, et al., Energy Mater. 1 (2021) 100013.
[34] Y. Yamada, J. Wang, S. Ko, E. Watanabe, A. Yamada, Nat. Energy 4 (2019) 269–280.
[35] J.F. Ding, R. Xu, N. Yao, et al., Angew. Chem. Int. Ed. 60 (2021) 11442–11447.
[36] F. Huang, L. Gao, Y. Zou, et al., J. Mater. Chem. A 7 (2019) 12498–12506.
[37] C.C. Su, M. He, R. Amine, K. Amine, Angew. Chem. Int. Ed. 58 (2019) 10591–10595.

[38] Z. Jiang, Z. Zeng, X. Liang, et al., Adv. Funct. Mater. 31 (2021) 2005991.
[39] Z. Jiang, Z. Zeng, B. Zhai, et al., J. Power Sources 506 (2021) 230086.
[40] D.J. Yoo, S. Yang, K.J. Kim, J.W. Choi, Angew. Chem. Int. Ed. 59 (2020) 14869–14876.
[41] C. Zhu, C. Sun, R. Li, et al., ACS Energy Lett. 7 (2022) 1338–1347.
[42] X. Peng, Y. Lin, Y. Wang, Y. Li, T. Zhao, Nano Energy 96 (2022) 107102.
[43] H. Zhang, Z. Zeng, R. He, et al., Energy Storage Mater. 48 (2022) 393–402.
[44] Z. Chen, B. Wang, Y. Li, et al., ACS Appl. Mater. Interfaces 14 (2022) 28014–28020.
[45] X.Q. Zhang, T. Li, B.Q. Li, et al., Angew. Chem. Int. Ed. 59 (2020) 3252–3257.
[46] X. Zheng, L. Huang, W. Luo, et al., ACS Energy Lett. 6 (2021) 2054–2063.
[47] A. Ramasubramanian, V. Yurkiv, T. Foroozan, et al., J. Phys. Chem. C 123 (2019) 10237–10245.